Original Article | Musculoskeletal Imaging

eISSN 2005-8330
https://doi.org/10.3348/kjr.2024.0912
Korean J Radiol 2025;26(6):581-592

Korean Journal of Radiology
KJR

Magnetic Resonance Imaging of the Peripheral Nerves and Fascicles of the Knee Using Double Echo Steady State Sequence at 7 Tesla

Pinzhen Chen[1]*, Zhiming Zhen[1]*, Jing Li[1], Taotao Yang[1], Wenjing Hou[1], Meng Zeng[1], Mingshan Du[1], Suyi Zhou[1], Wei Chen[2], Yicheng Hsu[3], Bo Wang[4], Zhi Liu[4], Yi Wu[5], Jiafei Chen[1], Wei Chen[1]

[1]Department of Radiology, 7T Magnetic Resonance Translational Medicine Research Center, Southwest Hospital, Army Medical University (Third Military Medical University), Chongqing, China
[2]The MR Research Collaboration Team, Siemens Healthineers Ltd., Wuhan, China
[3]The MR Research Collaboration Team, Siemens Healthineers Ltd., Shanghai, China
[4]Department of Neurosurgery, Southwest Hospital, Army Medical University (Third Military Medical University), Chongqing, China
[5]Department of Digital Medicine, College of Biomedical Engineering and Medical Imaging, Army Medical University, Chongqing, China

Objective: To evaluate the applicability of the double echo steady state (DESS) sequence at 7 tesla (7T) for high-resolution imaging of the peripheral nerves and fascicles of the knee.

Materials and Methods: We prospectively included 32 healthy participants (mean age 39 ± 14 years, 20 females). The patients underwent 7T magnetic resonance imaging (MRI) of the knee using proton density turbo spin-echo fat suppression (PD-TSE FS), three-dimensional DESS (3D-DESS), and higher in-plane resolution DESS ($DESS_{HR}$) sequences. The signal-to-noise ratios (SNRs) of the peroneal nerve (PN) and tibial nerve (TN) and contrast-to-noise ratios (CNRs) between the nerves and adjacent fat, vessels, and muscles were quantitatively measured by two readers and averaged. Five radiologists qualitatively assessed the overall image quality, pulsatile flow artifacts, and visualization of the PN and its branches, the TN, and the saphenous nerve (SN) using a five-point Likert-type scale, with the results averaged. The results of the three image sequences were compared.

Results: The SNR for the TNs in the $DESS_{HR}$ sequence were lower than those in the PD-TSE FS ($P < 0.001$) and 3D-DESS ($P = 0.024$) sequences, whereas the SNR for the PNs did not differ significantly across the three sequences. The $DESS_{HR}$ sequence exhibited superior TN- or PN-to-fat and PN-to-muscle CNR values when compared with the PD-TSE FS and 3D-DESS sequences ($P \leq 0.016$). The TN- and PN-to-vessel CNR values in the $DESS_{HR}$ and PD-TSE FS sequences were higher than those in the 3D-DESS sequence ($P \leq 0.001$). Qualitative assessments revealed fewer pulsatile artifacts in 3D-DESS than in $DESS_{HR}$ and PD-TSE FS ($P < 0.001$), with $DESS_{HR}$ exhibiting fewer artifacts than PD-TSE FS ($P = 0.035$). $DESS_{HR}$ excelled in visualizing the common PN, TN, and SN when compared with other sequences ($P < 0.001$), whereas 3D-DESS provided superior visualization of PN branches when compared with other sequences ($P \leq 0.042$).

Conclusion: The DESS sequence at 7T MRI enhances visualization of peripheral nerves and fascicular structures around the knee.

Keywords: 7 tesla; Magnetic resonance imaging; Double-echo steady-state sequence; Peripheral nerve; Knee

Received: August 10, 2024 **Revised:** March 18, 2025 **Accepted:** March 19, 2025

*These authors contributed equally to this work.

Corresponding author: Wei Chen, MD, Department of Radiology, 7T Magnetic Resonance Translational Medicine Research Center, Southwest Hospital, Army Medical University (Third Military Medical University), No. 30 Gaotanyan Street, Shapingba District, Chongqing 400038, China
• E-mail: landcw@tmmu.edu.cn
Corresponding author: Jiafei Chen, PhD, Department of Radiology, 7T Magnetic Resonance Translational Medicine Research Center, Southwest Hospital, Army Medical University (Third Military Medical University), No. 30 Gaotanyan Street, Shapingba District, Chongqing 400038, China
• E-mail: chenjiafei@tmmu.edu.cn

INTRODUCTION

The peroneal nerve (PN), tibial nerve (TN), and saphenous nerve (SN) are the primary peripheral nerves located in the vicinity of the knee joint and are vulnerable to injury from external forces [1-3] or surgical interventions, such as medial arthrotomy, meniscectomy, arthroscopic anterior cruciate ligament repair, and total knee replacement [4]. Damage to these nerves can cause various clinical symptoms such as pain, numbness, and impaired lower-extremity function [5]. Although ultrasonography is commonly employed for imaging peripheral nerves [6], its limited penetration makes it ineffective for visualizing small or deep-seated nerves, such as the sural and musculocutaneous or deeper branches of the PN, TN, and SN [7].

Magnetic resonance imaging (MRI) is a valuable tool for examining peripheral nerves and provides detailed information on neuropathy and the surrounding tissues [8,9]. Although 3 tesla (3T) MRI has been effective in observing larger nerves such as the common PN, TN, and sciatic nerve [10-14], it remains inadequate for smaller nerves and fascicles because of its limited spatial resolution. Our preliminary study also revealed suboptimal image quality for visualizing the SN, common PN at the fibula neck, as well as smaller branches of the peripheral nerve using proton density (PD) and double echo steady state (DESS) sequences at 3T MRI (Supplement, Supplementary Table 1, Supplementary Figs. 1-3). In contrast, 7T MRI offers a higher signal-to-noise ratio (SNR) and resolution [15], enabling more precise visualization of minute anatomical structures.

The DESS sequence, which incorporates water excitation technology for fat suppression (FS) [16], enhances the distinction between fat and other anatomical structures [17,18]. This sequence has been used to image the alveolar nerve [19], facial nerve [20], lumbosacral plexus [21], and upper extremity peripheral nerves [22] at 3T MRI. Additionally, previous studies have demonstrated its utility for visualizing the cervical nerve systems at 7T MRI [23,24]. However, the application of the three-dimensional (3D)-DESS sequence at 7T for visualizing the knee peripheral nerves remains unexplored. A comprehensive investigation into the utilization of this sequence is essential to maximize the capabilities of 7T MRI for visualizing the peripheral nerves and fascicular structures around the knee.

Peripheral nerves consist of numerous nerve bundles enveloped by connective tissue membranes, small blood vessels, and adipose tissue [25]. A previous study [26] employed the PD turbo spin-echo FS (PD-TSE FS) sequence at 7T to determine the axonal fascicle count in the median nerve. However, spin-echo imaging at 7T was compromised by ghosting artifacts from pulsatile flow, which hindered nerve visualization. Furthermore, the small size of the knee peripheral nerve bundles requires a high in-plane spatial resolution that is crucial for depicting fascicles and identifying pathological changes [27]. Thus, the objective of this study was to assess the applicability of the 7T DESS sequence for high-resolution imaging of the peripheral nerves and fascicular structures around the knee.

MATERIALS AND METHODS

Participants

This prospective study was approved by the Institutional Review Board of the local hospital (IRB No. KY2022147), and all participants provided written informed consent. From July 2022 to January 2024, healthy participants who met the inclusion and exclusion criteria were continuously enrolled based on the order of registration. The inclusion criteria were: healthy adults aged ≥20 years with a BMI of 18.5–28.0 kg/m^2 and no contraindications for MR examination. The exclusion criteria were: muscle disease; metabolic diseases; severe infections; heart, lung, liver, and kidney dysfunction; and life-threatening diseases or serious unstable underlying conditions posing a high risk for trial safety. The study included 38 healthy participants. Two participants who lacked PD-TSE FS images and four who showed severe motion artifacts were excluded from this study.

The final analysis included 32 participants.

MRI Acquisition

MR neurography data were prospectively acquired using a 7T scanner (MAGNETOM Terra, Siemens Healthineers, Erlangen, Germany) equipped with a 28-channel knee coil. The MRI protocols (Table 1) included acquisition of axial PD-TSE FS sequences and two three-dimensional (3D)-DESS sequences with different resolutions. Specifically, a sagittal DESS sequence with an isotropic resolution of 0.4 mm was employed for 3D structural evaluation, which was then reconstructed to the axial plane, and an axial DESS sequence with a resolution of 0.17 x 0.17 x 2 mm^3 ($DESS_{HR}$) was used to assess nerve fascicles. To standardize imaging protocols, all participants underwent MRI of the right knee.

During the testing phase, we fine-tuned the sampling

https://doi.org/10.3348/kjr.2024.0912

Korean Journal of Radiology
KJR

Table 1. MRI protocols at 7T

Parameter	PD-TSE FS	3D-DESS	$DESS_{HR}$
Image plane	Axial scan	Isotropic sagittal scan, with reconstruction into axial plane	Axial scan
Repetition time, msec	3200	15	15
Echo time, msec	32	4.48	4.48
Flip angle, °	180	28	20
Bandwidth, Hz/Px	139	250	249
FOV, mm^2	160 x 160	158 x 158	158 x 158
Averages	2	1	1
Matrix	800 x 800	400 x 400	912 x 912
Resolution, mm^3	0.2 x 0.2 x 2.5	0.4 x 0.4 x 0.4	0.17 x 0.17 x 2
Fat suppression	FS	WE	WE
Tubor factor	5	-	-
Acceleration factor	2	3	3
Partial Fourier factor	Off	Off	Off
Scan percentage, %	100	100	100
Number of slices	30	208	60
Time	8 min 40s	8 min 14s	8 min 2s

MRI = magnetic resonance imaging, 7T = 7 tesla, PD = proton density, TSE = turbo spin-echo, FS = fat suppression, 3D = three-dimensional, DESS = double echo steady state, $DESS_{HR}$ = means DESS sequence with a high in-plane resolution, FOV = field of view, WE = water excitation

perfection with application-optimized contrasts using different flip angle evolution (SPACE) and fast low-angle shot (FLASH) alongside DESS with an isotropic resolution of 0.4 mm^3 at 7T for imaging the peripheral nerves of the knee. Detailed images of these sequences are shown in Supplementary Figure 4. We found that the DESS sequence provided superior delineation of the PN and TN branches and effectively distinguished nerves and adjacent vessels when compared with the other sequences. Consequently, we selected DESS sequences for this study.

Imaging Analysis

The SNR of the nerves and contrast-to-noise ratios (CNRs) of nerve-to-fat, -vessel, and -muscle were calculated using region of interest (ROI) placed within the TN, PN, adjacent fat, popliteal vein, and gastrocnemius muscle on axial source images at the level of the popliteal fossa, as shown in Figure 1. These calculations were based on the mean signal intensity (SI) and standard deviation (SD), as per Equations (1) and (2):

$$SNR = \frac{Mean\ (SI_{nerve})}{Mean\ SD\ (SI_{air\ from\ four\ ROIs\ at\ the\ corners\ of\ the\ image})} \quad (1)$$

$$CNR = \frac{Mean\ (SI_{nerve}) - Mean\ (SI_{surrounding\ tissue})}{SD\ (SI_{surrounding\ tissue})} \quad (2)$$

In addition, because some nerve-to-muscle CNR values

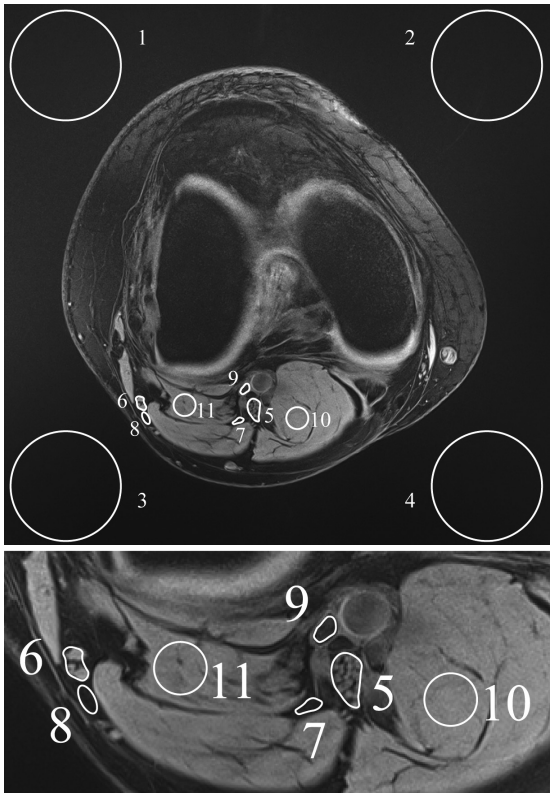

Fig. 1. Definition of ROIs for signal-to-noise ratio and contrast-to-noise ratio evaluation at the popliteal fossa level. The inner area of each ROI was evaluated, excluding the edges. Specifically, ROIs 1 to 4 measure noise levels. ROIs 5 and 6 measure tibial and peroneal nerves. ROIs 7 and 8 measure adjacent fat tissue, and ROI 9 measures the popliteal vein. ROIs 10 and 11 measure the gastrocnemius muscle signals. ROI = region of interest

https://doi.org/10.3348/kjr.2024.0912

were negative during the calculation, their absolute values were used to accurately represent the contrast magnitude ensuring consistent nerve-muscle differentiation assessment. The SNR and CNR values for the SN were not measured due to its small size, which resulted in insufficient visualization of certain 7T sequences. All ROIs of all participants were independently drawn by two radiologists (C.P.Z. and Z.Z.M., with 5 and 8 years of experience in radiology, respectively), and results from both measurements were used for further analysis.

A group of five radiologists (J.L., T.T.Y., W.J.H., M.Z., and M.S.D.), with 5–14 years of musculoskeletal MRI experience independently assessed the images without knowledge of the acquisition methodologies. Before evaluation, all patients received detailed instructions and training from a senior musculoskeletal radiologist (W.C., with 30 years of experience). The radiologists evaluated the overall image quality, pulsatile flow artifacts, and nerve segment visualization on axial source images spanning from the popliteal fossa to the PN branching level using a five-point Likert-type scale [28,29], as shown in Figure 2 and Table 2.

For evaluation, the PN was anatomically separated into a proximal segment (common PN) and a distal segment (branches of the PN, including the deep and superficial PNs and articular and muscular branches). The results from the five readers were averaged for further statistical analyses to compare the different sequences.

Statistical Analysis

The normality of the data distribution was verified using the Kolmogorov-Smirnov test. The summary of the data was presented as mean ± SD or median with interquartile range, accordingly. The SNR values of the nerves and the CNR values of the nerves-to-fat and -vessels exhibited a normal distribution. Therefore, a one-way repeated-measures ANOVA test was conducted to compare these measurements across the three sequences, with a post-hoc Bonferroni test used for multiple comparisons. The CNR values of the nerves-to-muscle and the qualitative measurements resulting from the five-point Likert scale did not conform to a normal distribution. Therefore, the differences in these measurements across the three sequences were evaluated using the Friedman test, followed by the pairwise post-hoc Wilcoxon test with Bonferroni-Holm correction to correct for multiple comparisons.

The interrater agreement between the two readers in measuring the SNR and CNR values was calculated using intraclass correlation coefficients (ICCs) employing a two-way mixed absolute agreement model. The interrater agreement among the five readers for qualitative

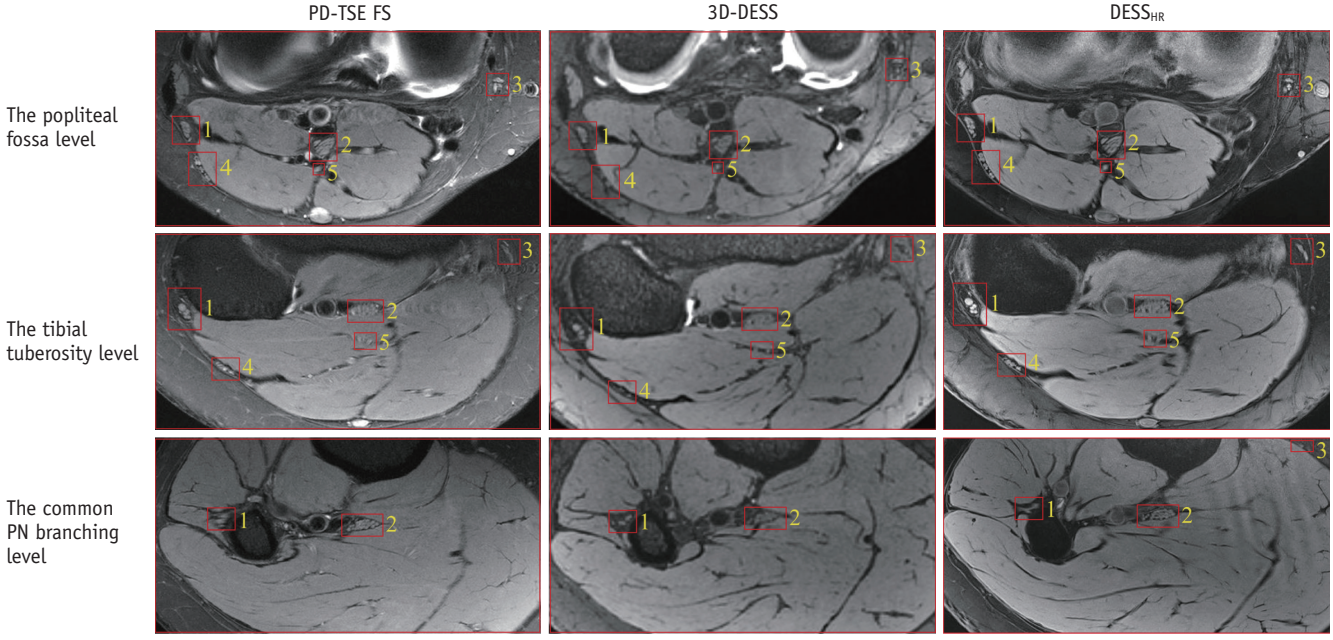

Fig. 2. A comparison of axial PD-TSE FS, 3D-DESS, and $DESS_{HR}$ images at 7T MR in a 29-year-old healthy female, focusing on peripheral nerves at different knee levels. PN (label 1), tibial nerve (label 2), saphenous nerve (label 3), lateral sural cutaneous nerve (label 4), and tibial nerve muscular branches (label 5). PD = proton density, TSE = turbo spin-echo, FS = fat suppression, 3D = three-dimensional, DESS = double echo steady state, $DESS_{HR}$ = means DESS sequence with a high in-plane resolution, 7T = 7 tesla, MR = magnetic resonance, PN = peroneal nerve

https://doi.org/10.3348/kjr.2024.0912

Korean Journal of Radiology
KJR

Table 2. Criteria for the 5-point Likert scale gradings

Variables	5-point Likert scale
Overall image quality	1. Non-diagnostic quality 2. Poor image quality 3. Acceptable image quality 4. Good image quality 5. Excellent image quality enables precise differentiation between muscle tissue and adjacent fascia/septum. The muscle signal is consistently homogeneous across the visual field
Pulsatile flow artifacts	1. Severe pulsatile flow artifacts: these artifacts severely hinder the evaluation of all nerve structures 2. Visible pulsatile flow artifacts with high signal intensity: these artifacts moderately interfere with the assessment of two adjacent nerve types 3. Moderate pulsatile flow artifacts: these artifacts slightly obstruct the assessment of adjacent nerves 4. Visible pulsatile flow artifacts with mild signal intensity: these artifacts do not impede the evaluation of adjacent nerves 5. None
Visualization of the tibial nerve and the common peroneal nerve	1. Non-diagnostic: characterized by extensive blurring that precludes accurate interpretation 2. Poor: nerve borders and anatomical details are poorly visualized, making clear delineation difficult 3. Moderate: nerve borders are visible with some blurring into surrounding tissues; individual nerve fascicles appear blurred and indistinguishable from one another 4. Good: nerve borders are well visualized with minimal blurring; anatomical depiction includes clear visualization of several individual nerve fascicles 5. Excellent: nerve borders and fascicular structures are sharply delineated, allowing for clear differentiation between individual fascicles
Visualization of the branches of the peroneal nerve	1. Non-diagnostic: characterized by extensive blurring that precludes accurate interpretation 2. Poor: the deep peroneal nerve, superficial peroneal nerve, articular branch, and muscular branch nerve borders are poorly visualized 3. Moderate: the deep peroneal and superficial peroneal nerve borders are moderately visible with some blurring into surrounding tissues; the articular branch and muscular branch nerves are not distinguishable 4. Good: the deep peroneal and superficial peroneal nerve borders are well visualized; however, the articular branch and muscular branch nerves exhibit some blurring 5. Excellent: all branches of the peroneal nerve, including the deep peroneal, superficial peroneal, articular branch, and muscular branch nerves, are clearly and perfectly delineated
Visualization of the saphenous nerve	1. None: no visualization of the saphenous nerve 2. Poor: visualization is hindered by extensive blurring, making the saphenous nerve indistinct 3. Moderate: the borders of the saphenous nerve are moderately visible, but the distal saphenous nerve cannot be identified 4. Good: both proximal and distal saphenous nerve borders are well visualized with minor blurring 5. Excellent: the saphenous nerve borders and fascicular structures are clearly and perfectly delineated

measurements was calculated using Fleiss Kappa [30,31]. Kappa values of 0.41–0.60, 0.61–0.80, and 0.81–1.0 indicated moderate, substantial, and almost perfect interrater agreement, respectively.

Statistical significance was set at $P < 0.05$, and computations were conducted using IBM SPSS Statistics for Windows, version 26.0. (IBM Corp., Armonk, NY, USA). Graphs were generated using GraphPad Prism, version 10 (GraphPad Software Inc., La Jolla, CA, USA).

RESULTS

Participant Characteristics

This study ultimately included 32 healthy individuals (20 females, 12 males) with a mean age of 39 ± 14 years and a BMI of 22.2 ± 2.6 kg/m^2.

Interrater Reliability

The ICCs for the SNR and CNR values ranged from 0.897–0.994. The interrater agreement for assessing qualitative measurements across all five readers ranged from 0.644 to

 https://doi.org/10.3348/kjr.2024.0912

0.813 (Table 3).

SNR and CNR Values

The SNR and CNR values for the TN and PN were compared across the different sequences (Fig. 2, Table 4). The SNR for the TN in the $DESS_{HR}$ sequence was lower than that in the PD-TSE FS ($P < 0.001$) and 3D-DESS ($P = 0.024$) sequences. We detected no significant differences in the SNR of the PN across all sequences ($P = 0.387$).

Table 3. The interobserver agreement results of SNR, CNR, and qualitative data

Quantitative data	ICC	95% CI	*P*
SNR	0.994	0.991–0.996	<0.001
CNR nerve to fat	0.954	0.904–0.974	<0.001
CNR nerve to vessel	0.897	0.824–0.935	<0.001
CNR nerve to muscle	0.937	0.828–0.970	<0.001
Qualitative data	**Fleiss kappa**	**95% CI**	***P***
Overall image quality	0.751	0.749–0.753	<0.001
Pulsatile flow artifacts	0.813	0.811–0.814	<0.001
CPN visualization	0.744	0.742–0.745	<0.001
BPN visualization	0.644	0.643–0.646	<0.001
TN visualization	0.743	0.742–0.744	<0.001
SN visualization	0.788	0.787–0.789	<0.001

SNR = signal-to-noise ratio, CNR = contrast-to-noise ratio, ICC = intraclass correlation coefficient, CI = confidence interval, CPN = common peroneal nerve, BPN = branches of the peroneal nerve, TN = tibial nerve, SN = saphenous nerve

Regarding the CNR of nerves-to-fat, the CNRs of TN-to-fat and PN-to-fat of the $DESS_{HR}$ sequence were higher than those of the PD-TSE FS and 3D-DESS sequences ($P < 0.001$). Regarding the CNR of nerves-to-vessels, the CNRs of TN-to-vessel and PN-to-vessel of the PD-TSE FS sequence were higher than those of the 3D-DESS ($P < 0.001$). Moreover, the CNR of TN-to-vessel of the PD-TSE FS sequence was higher than that of the $DESS_{HR}$ sequence ($P = 0.014$). However, the $DESS_{HR}$ and PD-TSE FS sequences showed no significant differences in the CNR of the PN-to-vessel ($P > 0.99$). The CNRs of the TN-to-vessel and PN-to-vessel of the $DESS_{HR}$ sequence were higher than those of the 3D-DESS sequence ($P < 0.001$). And with respect to the CNR of nerves-to-muscle, the $DESS_{HR}$ sequence provided higher CNR of PN-to-muscle than the other sequences ($P = 0.010$ vs. PD-TSE FS, $P = 0.016$ vs. 3D-DESS). No significant differences were found between the other nerve-to-muscle CNR values ($P > 0.05$).

Qualitative Analysis

Qualitative analysis compared the three sequences at 7T MR (Fig. 3, Table 5). The 3D-DESS and $DESS_{HR}$ sequences demonstrated superior image quality when compared with the PD-TSE FS sequence ($P < 0.001$), with no significant difference observed between the 3D-DESS and $DESS_{HR}$ sequences ($P > 0.99$). The 3D-DESS sequence exhibited fewer pulsatile flow artifacts than the PD-TSE FS and $DESS_{HR}$

Table 4. The SNR value of peripheral nerves and the CNR values of peripheral nerves to tissue in different sequences at 7T MRI

	PD-TSE FS	3D-DESS	$DESS_{HR}$	3D-DESS vs. PD-TSE FS	$DESS_{HR}$ vs. PD-TSE FS	$DESS_{HR}$ vs. 3D-DESS
SNR						
TN	64.7 ± 17.0	57.1 ± 15.2	48.2 ± 15.1	0.036*	<0.001*	0.024*
PN	71.9 ± 19.3	74.7 ± 18.0	69.9 ± 21.1	NS*	NS*	NS*
CNR nerve-fat						
TN	5.6 ± 2.6	4.8 ± 2.4	13.0 ± 5.1	0.720*	<0.001*	<0.001*
PN	7.7 ± 2.6	8.2 ± 3.9	17.8 ± 6.4	1*	<0.001*	<0.001*
CNR nerve-vessel						
TN	15.4 ± 6.9	6.1 ± 4.7	11.3 ± 4.7	<0.001*	0.014*	0.001*
PN	17.5 ± 8.6	9.7 ± 5.7	18.0 ± 6.7	<0.001*	1*	<0.001*
CNR nerve-muscle						
TN	1.9 (1.3, 3.3)	2.5 (1.0, 4.1)	2.2 (1.1, 3.4)	NS†	NS†	NS†
PN	1.8 (1.1, 3.3)	2.3 (1.7, 2.91)	4.0 (2.2, 6.4)	1†	0.010†	0.016†

Data is mean ± standard deviation or median (interquartile range).
*Means of the repeated-measures ANOVA test with post hoc analysis using the Bonferroni test were employed, †Means of the Friedman test with pairwise post hoc Wilcoxon test with Bonferroni-Holm correction were employed. $P < 0.05$ means a significant difference. With the *P*-values of 0.387 for SNR (from repeated-measures ANOVA) and 0.552 for CNR nerve-muscle (from the Friedman test).
SNR = signal-to-noise ratio, CNR = contrast-to-noise ratio, 7T = 7 tesla, MRI = magnetic resonance imaging, PD = proton density, TSE = turbo spin-echo, FS = fat suppression, 3D = three-dimensional, DESS = double echo steady state, $DESS_{HR}$ = means DESS sequence with a high in-plane resolution, TN = tibial nerve, PN = peroneal nerve, NS = not significant

https://doi.org/10.3348/kjr.2024.0912

Korean Journal of Radiology
KJR

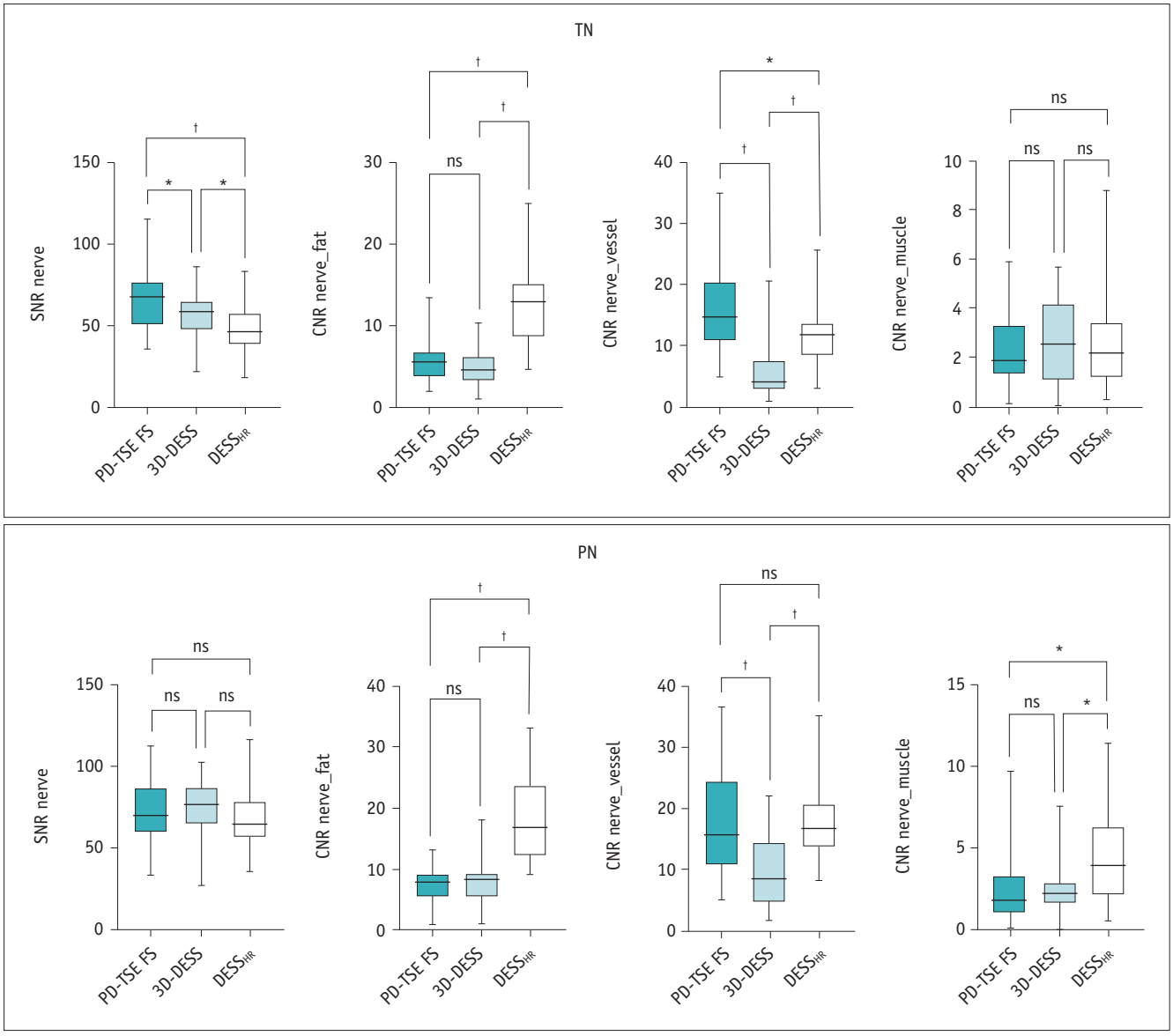

Fig. 3. Box and whisker plots summarize the SNR and CNR values across PD-TSE FS, 3D-DESS, and $DESS_{HR}$ sequences. Whiskers indicate minimum and maximum values. The repeated-measures ANOVA test compared the SNR and the CNR of nerves-to-fat and nerves- to-vessel across three sequences. The Friedman test compared the CNR of nerves-to-muscle. Statistical significance is indicated on a level of $^{*}P < 0.05$, $^{\dagger}P \leq 0.001$. All given *P*-values are adjusted for multiple comparisons. SNR = signal-to-noise ratio, CNR = contrast-to-noise ratio, PD = proton density, TSE = turbo spin-echo, FS = fat suppression, 3D = three-dimensional, DESS = double echo steady state, $DESS_{HR}$ = means DESS sequence with a high in-plane resolution, TN = tibial nerve, ns = not significant, PN = peroneal nerve

sequences ($P < 0.001$), and the $DESS_{HR}$ sequence presented fewer artifacts than the PD-TSE FS sequence ($P = 0.035$). Regarding nerve segment visualization (Fig. 4), the $DESS_{HR}$ sequence showed superior visualization of the CPN, TN, and SN when compared with the PD-TSE FS and 3D-DESS sequences ($P < 0.001$). The PD-TSE FS sequence showed superior TN and SN visualization when compared with the 3D-DESS sequence ($P < 0.001$), without a significant difference in CPN visualization ($P = 0.280$). However, branches of the peroneal nerve (BPN) were better visualized in the 3D-DESS sequence than in the PD-TSE FS ($P < 0.001$) and $DESS_{HR}$ ($P = 0.042$) sequences (Fig. 5).

DISCUSSION

Peripheral nerve imaging around the knee has long posed challenges at 3T MRI due to suboptimal image quality. Advanced 7T MRI holds promise for enhanced nerve

https://doi.org/10.3348/kjr.2024.0912

Table 5. Qualitative analysis for PD-TSE FS, 3D-DESS, $DESS_{HR}$ sequences at 7T MRI as assessed by five readers

Sequence	PD-TSE FS	3D-DESS	$DESS_{HR}$	*P*-values		
				3D-DESS vs. PD-TSE FS	$DESS_{HR}$ vs. PD-TSE FS	$DESS_{HR}$ vs. 3D-DESS
Overall image quality	4.2 (4.0–4.8)	5 (5.0–5.0)	5 (5.0–5.0)	<0.001	<0.001	1.000
Pulsatile flow artifacts	4 (3.2–4.0)	5 (5.0–5.0)	4 (4.0–4.0)	<0.001	0.035	<0.001
CPN visualization	4 (4.0–4.2)	4 (3.8–4.0)	5 (4.8–5.0)	0.280	<0.001	<0.001
BPN visualization	3.2 (3.0–3.4)	5 (4.2–5.0)	4.2 (4.0–4.6)	<0.001	<0.001	0.042
TN visualization	4 (4.0–4.0)	3.6 (3.2–4.0)	5 (5.0–5.0)	0.017	<0.001	<0.001
SN visualization	3.2 (3.0–4.0)	2 (2.0–2.0)	5 (4.8–5.0)	<0.001	<0.001	<0.001

Data were presented as the median (IQR) of the average values derived from the five grades assigned by the five readers. The Friedman test with pairwise post-hoc Wilcoxon test with Bonferroni-Holm correction was employed. $P < 0.05$ means a significant difference.
PD = proton density, TSE = turbo spin-echo, FS = fat suppression, 3D = three-dimensional, DESS = double echo steady state, $DESS_{HR}$ = means DESS sequence with a high in-plane resolution, 7T = 7 tesla, MRI = magnetic resonance imaging, IQR = interquartile range, CPN = common peroneal nerve, BPN = branches of the peroneal nerve, TN = tibial nerve, SN = saphenous nerve

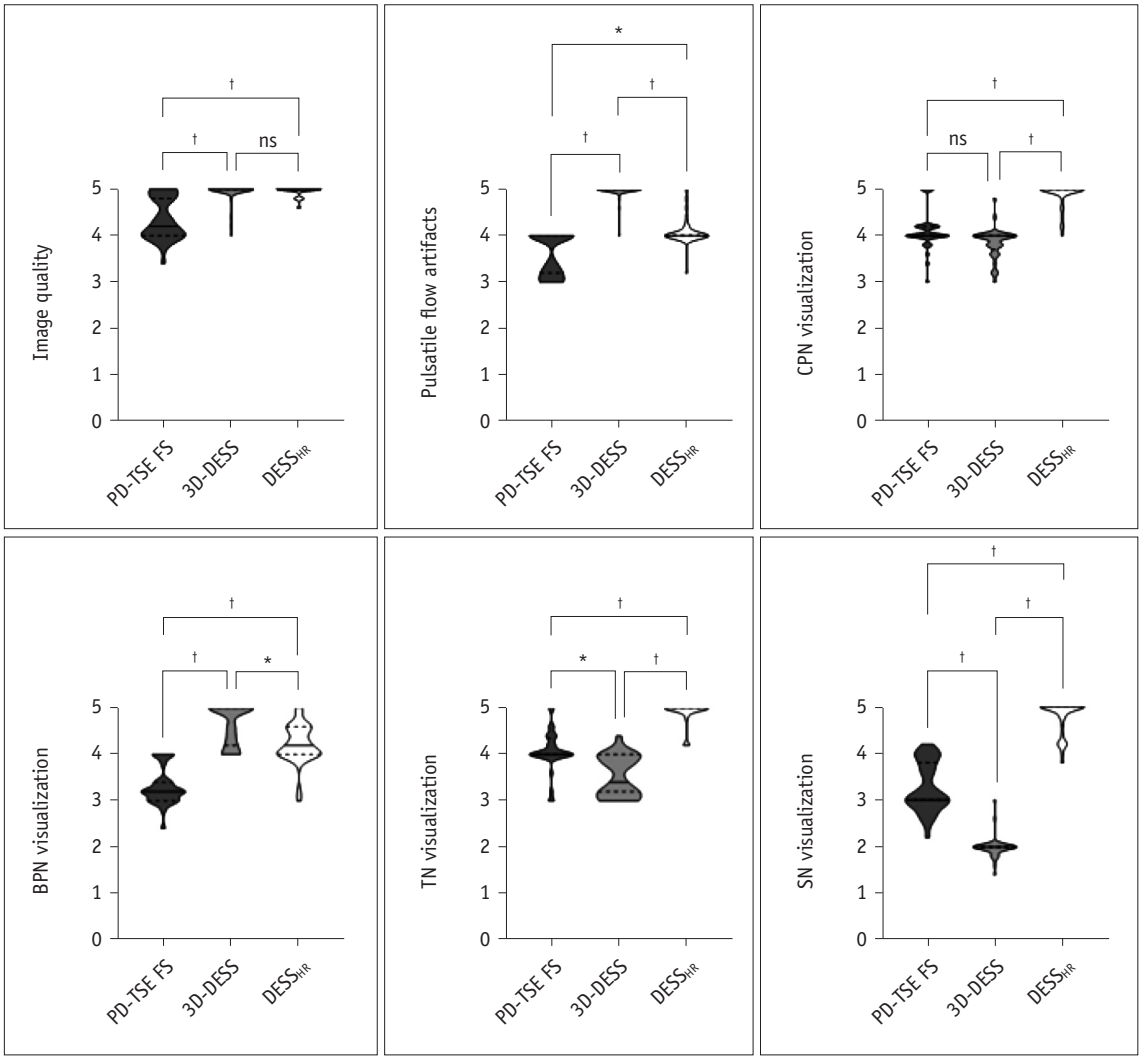

Fig. 4. Violin plots show the comparison of five Likert-type scale scores across PD-TSE FS, 3D-DESS, and $DESS_{HR}$ sequences. The solid lines represent the median and the dashed lines indicate the interquartile range. The Friedman test compared these measurements across three sequences. Statistical significance is indicated on a level of $^{*}P < 0.05$, $^{\dagger}P \leq 0.001$. All given *P*-values are adjusted for multiple comparisons. PD = proton density, TSE = turbo spin-echo, FS = fat suppression, 3D = three-dimensional, DESS = double echo steady state, $DESS_{HR}$ = means DESS sequence with a high in-plane resolution, ns = not significant, CPN = common peroneal nerve, BPN = branches of the peroneal nerve, TN = tibial nerve, SN = saphenous nerve

https://doi.org/10.3348/kjr.2024.0912

Korean Journal of Radiology
KJR

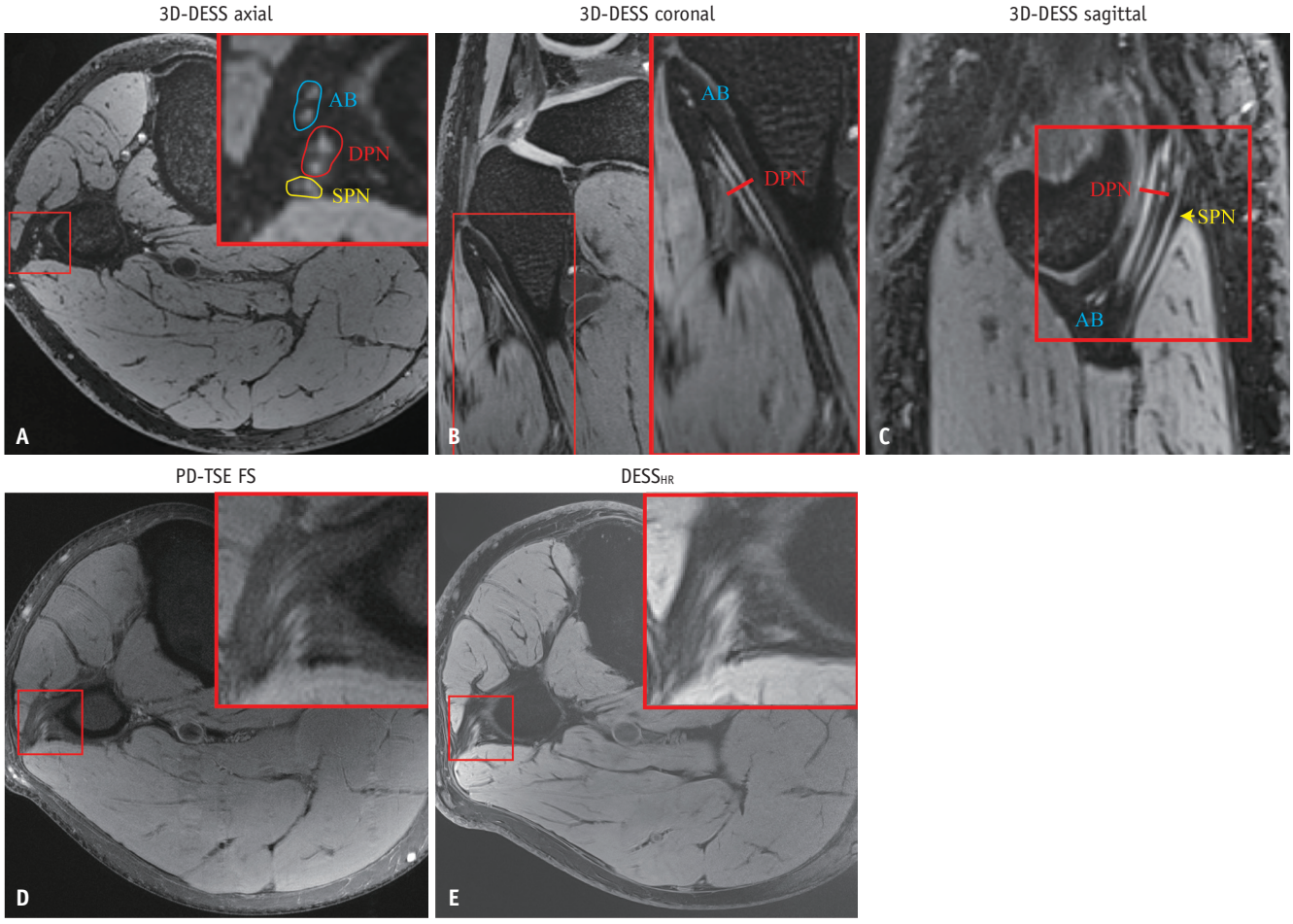

Fig. 5. Image of a 30-year-old male. Red boxes indicate a close-up of BPN region. The reconstructed 3D-DESS images in the axial, coronal, and sagittal planes show that the peroneal nerve is divided into the AB, DPN, and SPN. Furthermore, the visualization of the BPN in the 3D-DESS images **(A-C)** is superior to that in the axial PD-TSE FS **(D)** and $DESS_{HR}$ **(E)** images. BPN = branches of the peroneal nerve, 3D = three-dimensional, DESS = double echo steady state, AB = articular branch, DPN = deep peroneal nerve, SPN = superficial peroneal nerve, PD = proton density, TSE = turbo spin-echo, FS = fat suppression, $DESS_{HR}$ = means DESS sequence with a high in-plane resolution

visualization; however, studies investigating its applicability remain insufficient. This study demonstrates the potential of 7T MRI for imaging the peripheral nerves and fascicular structures around the knee. Specifically, the $DESS_{HR}$ sequence at 7T, with an in-plane resolution of 0.17 x 0.17 mm^2, improved the visualization of the TN, common PN, SN, and intricate fascicular structures. Additionally, the 3D-DESS sequence with 0.4 mm^3 isotropic resolution excelled in delineating and reconstructing smaller PN branches.

Our findings showed that while the SNR for the TN in the $DESS_{HR}$ sequence was lower than that in the PD-TSE FS and 3D-DESS sequences, the SNR differences for other nerves among the sequences were statistically insignificant. Three sequence protocols were optimized for comparable SNR and scan times, thus maximizing the image quality. An enhanced CNR plays a crucial role in nerve visualization [32]. The $DESS_{HR}$ sequence achieved higher nerve-to-fat contrast ratios, likely due to a decrease in the flip angle compared to the 3D-DESS sequence, which reduced T1 weighting, lowered fat signal brightness, and enhanced nerve signals. This led to a clearer delineation of the nerves, particularly the distal branch nerves. Notably, the CNR of the TN-to-fat was significantly lower than that of the PN-to-fat in both DESS sequences, suggesting heterogeneous FS. This discrepancy may arise from the DESS sequence's selective excitation of water protons FS, which is sensitive to B0 inhomogeneities at 7T [15].

The separation of nerves from adjacent vessels is challenging in MR neurography [33]. In this study, PD and $DESS_{HR}$ images demonstrated high CNR values from the nerves to the vessels. Vascular suppression and the higher spatial resolution of the PD and $DESS_{HR}$ images

https://doi.org/10.3348/kjr.2024.0912

at 7T enhanced the distinction between the vessels and peripheral nerves. Nerves typically exhibit a uniform intermediate SI, whereas the accompanying vessel walls exhibit an intermediate SI. The popliteal, anterior tibial, posterior tibial, and peroneal arteries and veins exhibited low or intermediate SI.

Additionally, we found that DESS images were less affected by ghosting pulsatile flow artifacts than PD-TSE FS images. This is likely due to the longer relaxation times and stronger phase-coding gradients in the PD sequence [15]. Conversely, the DESS sequence is insensitive to motion, and flow-induced displacement can attenuate the signal from flowing fluids, such as cerebrospinal fluid and blood vessels [21,34]. Furthermore, 3D scanning has the potential to reduce pulsatile motion artifacts when compared with 2D scanning. We also observed that the PD images were frequently accompanied by tissue signal inhomogeneity and instability in some slices, whereas these phenomena were absent in the DESS images. This may have occurred because B1 inhomogeneity is most prominent for current 2D spin echo, followed by 3D spin echo, and then 3D gradient echo-based imaging [15]. The DESS sequence exhibited diminished susceptibility to SI variation and pulsatile flow artifacts, thereby enhancing the overall image quality.

Notably, a high spatial resolution is crucial for visualizing nerve fascicles. The $DESS_{HR}$ sequence at 7T provided exceptional detail in visualizing individual nerve fascicles of the PN, TN, and SN, surpassing the PD-TSE FS sequence. This level of resolution is essential for diagnosing subtle neuropathic lesions affecting individual fascicles. Moreover, the $DESS_{HR}$ sequence achieved this detail with a shorter acquisition time than that reported in previous 7T MRI studies with similar resolution [35,36]. Remarkably, while the 3D-DESS sequence did not outperform the PD-TSE FS and $DESS_{HR}$ sequences for SN and TN visualization, it excelled in depicting smaller PN branches such as articular and muscular branches [37]. Previous cadaver studies focused on the anatomical relationship between the PN and its branches with the proximal fibula to aid in surgical preparation [3,38]. However, visualizing these fine structures in vivo using the 3D-DESS sequence at 7T is clinically significant, especially for presurgical planning and reducing nerve injury during knee procedures, given the variability in individual nerve paths [3].

This study had several limitations. First, it lacked data on diagnostic performance across various nerve pathologies. Investigating the utility of the DESS sequence for different forms of peripheral neuropathy is crucial for future research. Second, we did not evaluate the individual SNR and CNR values for different slices of the peripheral nerves. Noise in MR images may not be uniformly distributed because of parallel imaging and B1 inhomogeneity, potentially affecting the accuracy of the SNR and CNR calculations. Third, while the DESS sequences at 7T offer superior visualization of nerve segments, the increased acquisition time may limit their clinical feasibility. Future research could explore deep-learning reconstruction techniques that enhance spatial resolution, leverage knowledge of local noise distribution, and locally adapt the strength to address noise variations in 7T MR while avoiding long scan times.

In conclusion, the $DESS_{HR}$ sequence at 7T demonstrated superior contrast for visualizing peripheral nerves around the knee and provided detailed anatomical information on the nerve fascicular architecture. Moreover, the 3D-DESS sequence at 7T improved the visualization of the smaller and distal PN segments.

Supplement

The Supplement is available with this article at https://doi.org/10.3348/kjr.2024.0912.

Availability of Data and Material

The datasets generated or analyzed during the study are available from the corresponding author on reasonable request.

Conflicts of Interest

The authors have no potential conflicts of interest to disclose.

Author Contributions

Conceptualization: Jiafei Chen, Wei Chen. Data curation: Pinzhen Chen, Zhiming Zhen, Zhi Liu, Bo Wang. Formal analysis: Pinzhen Chen. Funding acquisition: Jiafei Chen. Investigation: Pinzhen Chen, Zhiming Zhen, Jing Li. Methodology: Pinzhen Chen, Zhiming Zhen, Wei Chen, Yicheng Hsu, Yi Wu. Project administration: Jiafei Chen, Wei Chen. Resources: Taotao Yang, Meng Zeng, Suyi Zhou. Software: Pinzhen Chen. Supervision: Wei Chen. Validation: Jiafei Chen, Wei Chen. Visualization: Jing Li, Wenjing Hou, Mingshan Du. Writing—original draft: Pinzhen Chen, Zhiming Zhen. Writing—review & editing: Jiafei Chen, Wei Chen, Yi Wu.

Korean Journal of Radiology
KJR

ORCID IDs
Pinzhen Chen
https://orcid.org/0000-0001-5013-1402
Zhiming Zhen
https://orcid.org/0000-0001-6064-1916
Jing Li
https://orcid.org/0000-0002-9438-0010
Taotao Yang
https://orcid.org/0009-0006-9933-9611
Wenjing Hou
https://orcid.org/0000-0003-1583-6786
Meng Zeng
https://orcid.org/0009-0009-5605-6496
Mingshan Du
https://orcid.org/0000-0003-4716-7791
Suyi Zhou
https://orcid.org/0009-0003-6129-6191
Wei Chen
https://orcid.org/0009-0005-2270-3166
Yicheng Hsu
https://orcid.org/0000-0002-7941-7639
Bo Wang
https://orcid.org/0000-0001-7066-2008
Zhi Liu
https://orcid.org/0009-0007-9658-255X
Yi Wu
https://orcid.org/0000-0002-2322-6825
Jiafei Chen
https://orcid.org/0000-0002-2511-4798
Wei Chen
https://orcid.org/0000-0002-6829-9067

Funding Statement
Supported by Chong Qing Natural Science Foundation (CSTB2023NSCQ-MSX0919).

Acknowledgments
The authors thank Zhuoli Zhang, PhD, Department of Radiological Sciences, University of California, USA, for the design and guidance of this study.

REFERENCES

1. Reddy CG, Amrami KK, Howe BM, Spinner RJ. Combined common peroneal and tibial nerve injury after knee dislocation: one injury or two? An MRI-clinical correlation. *Neurosurg Focus* 2015;39:E8
2. Chang KV, Mezian K, Naňka O, Wu WT, Lou YM, Wang JC, et al. Ultrasound imaging for the cutaneous nerves of the extremities and relevant entrapment syndromes: from anatomy to clinical implications. *J Clin Med* 2018;7:457
3. Hohmann E, Van Zyl R, Glatt V, Tetsworth K, Keough N. The anatomical relationship of the common peroneal nerve to the proximal fibula and its clinical significance when performing fibular-based posterolateral reconstructions. *Arch Orthop Trauma Surg* 2021;141:437-445
4. Becciolini M, Pivec C, Riegler G. Ultrasound imaging of the deep peroneal nerve. *J Ultrasound Med* 2021;40:821-838
5. Fisse AL, Katsanos AH, Gold R, Krogias C, Pitarokoili K. Cross-sectional area reference values for peripheral nerve ultrasound in adults: a systematic review and meta-analysis—part II: lower extremity nerves. *Eur J Neurol* 2021;28:2313-2318
6. Pirri C, Stecco C, Petrelli L, Macchi V, Özçakar L. Ultrasound imaging, anatomy and histology of nerves and fasciae: they never walk alone. *Int J Clin Pract* 2021;75:e13956
7. Möller I, Miguel M, Bong DA, Zaottini F, Martinoli C. The peripheral nerves: update on ultrasound and magnetic resonance imaging. *Clin Exp Rheumatol* 2018;36:145-158
8. Oudeman J, Eftimov F, Strijkers GJ, Schneiders JJ, Roosendaal SD, Engbersen MP, et al. Diagnostic accuracy of MRI and ultrasound in chronic immune-mediated neuropathies. *Neurology* 2020;94:e62-e74
9. Kavolus JJ, Sia D, Potter HG, Attarian DE, Lachiewicz PF. Saphenous nerve block from within the knee is feasible for TKA: MRI and cadaveric study. *Clin Orthop Relat Res* 2018;476:30-36
10. Foesleitner O, Sulaj A, Sturm V, Kronlage M, Godel T, Preisner F, et al. Diffusion MRI in peripheral nerves: optimized b values and the role of non-Gaussian diffusion. *Radiology* 2022;302:153-161
11. Chen Y, Baraz J, Xuan SY, Yang X, Castoro R, Xuan Y, et al. Multiparametric quantitative MRI of peripheral nerves in the leg: a reliability study. *J Magn Reson Imaging* 2024;59:563-574
12. Fortanier E, Ogier AC, Delmont E, Lefebvre MN, Viout P, Guye M, et al. Quantitative assessment of sciatic nerve changes in Charcot-Marie-Tooth type 1A patients using magnetic resonance neurography. *Eur J Neurol* 2020;27:1382-1389
13. Kumar S, Mangi MD, Zadow S, Lim W. Nerve entrapment syndromes of the lower limb: a pictorial review. *Insights Imaging* 2023;14:166
14. Sneag DB, Zochowski KC, Tan ET, Queler SC, Burge A, Endo Y, et al. Denoising of diffusion MRI improves peripheral nerve conspicuity and reproducibility. *J Magn Reson Imaging* 2020;51:1128-1137
15. Pazahr S, Nanz D, Sutter R. 7 T musculoskeletal MRI: fundamentals and clinical implementation. *Invest Radiol* 2023;58:88-98
16. Bruder H, Fischer H, Graumann R, Deimling M. A new steady-state imaging sequence for simultaneous acquisition of two MR images with clearly different contrasts. *Magn Reson Med* 1988;7:35-42
17. Norman B, Pedoia V, Majumdar S. Use of 2D U-Net

 https://doi.org/10.3348/kjr.2024.0912

convolutional neural networks for automated cartilage and meniscus segmentation of knee MR imaging data to determine relaxometry and morphometry. *Radiology* 2018;288:177-185
18. Chaudhari AS, Stevens KJ, Sveinsson B, Wood JP, Beaulieu CF, Oei EHG, et al. Combined 5-minute double-echo in steady-state with separated echoes and 2-minute proton-density-weighted 2D FSE sequence for comprehensive whole-joint knee MRI assessment. *J Magn Reson Imaging* 2019;49:e183-e194
19. Al-Haj Husain A, Stadlinger B, Winklhofer S, Müller M, Piccirelli M, Valdec S. Mandibular third molar surgery: intraosseous localization of the inferior alveolar nerve using 3D double-echo steady-state MRI (3D-DESS). *Diagnostics (Basel)* 2021;11:1245
20. Jeong HS, Kim Y, Kim HJ, Kim HJ, Kim EH, Woo SY, et al. Imaging of facial nerve with 3D-DESS-WE-MRI before parotidectomy: impact on surgical outcomes. *Korean J Radiol* 2023;24:860-870
21. Lin Y, Tan ET, Campbell G, Colucci PG, Singh S, Lan R, et al. Improved 3D DESS MR neurography of the lumbosacral plexus with deep learning and geometric image combination reconstruction. *Skeletal Radiol* 2024;53:1529-1539
22. Campbell GJ, Sneag DB, Queler SC, Lin Y, Li Q, Tan ET. Quantitative double echo steady state T2 mapping of upper extremity peripheral nerves and muscles. *Front Neurol* 2024;15:1359033
23. Feuerriegel GC, Marth AA, Germann C, Wanivenhaus F, Nanz D, Sutter R. 7 T MRI of the cervical neuroforamen: assessment of nerve root compression and dorsal root ganglia in patients with radiculopathy. *Invest Radiol* 2024;59:450-457
24. Galley J, Sutter R, Germann C, Wanivenhaus F, Nanz D. High-resolution in vivo MR imaging of intraspinal cervical nerve rootlets at 3 and 7 tesla. *Eur Radiol* 2021;31:4625-4633
25. Chen Y, Haacke EM, Li J. Peripheral nerve magnetic resonance imaging. *F1000Res* 2019;8:1803
26. Riegler G, Drlicek G, Kronnerwetter C, Heule R, Bieri O, Bodner G, et al. High-resolution axonal bundle (fascicle) assessment and triple-echo steady-state T2 mapping of the median nerve at 7 T: preliminary experience. *Invest Radiol* 2016;51:529-535
27. Snoj Ž, Serša I, Matičič U, Cvetko E, Omejec G. Nerve fascicle depiction at MR microscopy and high-frequency us with anatomic verification. *Radiology* 2020;297:672-674
28. Heiss R, Weber MA, Balbach E, Schmitt R, Rehnitz C, Laqmani A, et al. Clinical application of ultrahigh-field-strength wrist MRI: a multireader 3-T and 7-T comparison study. *Radiology* 2023;307:e220753
29. Preisner F, Hayes JC, Charlet T, Carinci F, Hielscher T, Schwarz D, et al. Simultaneous multislice accelerated TSE for improved spatiotemporal resolution and diagnostic accuracy in magnetic resonance neurography: a feasibility study. *Invest Radiol* 2023;58:363-371
30. Han K, Ryu L. Statistical methods for the analysis of inter-reader agreement among three or more readers. *Korean J Radiol* 2024;25:325-327
31. Choi KS, Park C, Lee JY, Lee KH, Jeon YH, Hwang I, et al. Prospective evaluation of accelerated brain MRI using deep learning-based reconstruction: simultaneous application to 2D spin-echo and 3D gradient-echo sequences. *Korean J Radiol* 2025;26:54-64
32. Ensle F, Kaniewska M, Tiessen A, Lohezic M, Getzmann JM, Guggenberger R. Diagnostic performance of deep learning-based reconstruction algorithm in 3D MR neurography. *Skeletal Radiol* 2023;52:2409-2418
33. Pedrick EG, Sneag DB, Colucci PG, Duong M, Tan ET. Three-dimensional MR neurography of the brachial plexus: vascular suppression with low-dose ferumoxytol. *Radiology* 2023;307:e221087
34. Qin Y, Zhang J, Li P, Wang Y. 3D double-echo steady-state with water excitation MR imaging of the intraparotid facial nerve at 1.5T: a pilot study. *AJNR Am J Neuroradiol* 2011;32:1167-1172
35. Yoon D, Biswal S, Rutt B, Lutz A, Hargreaves B. Feasibility of 7T MRI for imaging fascicular structures of peripheral nerves. *Muscle Nerve* 2018;57:494-498
36. Sveinsson B, Rowe OE, Stockmann JP, Park DJ, Lally PJ, Rosen MS, et al. Feasibility of simultaneous high-resolution anatomical and quantitative magnetic resonance imaging of sciatic nerves in patients with Charcot-Marie-Tooth type 1A (CMT1A) at 7T. *Muscle Nerve* 2022;66:206-211
37. Grechenig P, Hohenberger G, Maier M, Grechenig C, Holweg P, Vielgut I, et al. The articular branch of the peroneal nerve to the proximal tibiofibular joint descends at a mean height of approximately 18 mm distal to the postero-lateral tip of the fibular head. *Knee Surg Sports Traumatol Arthrosc* 2021;29:1232-1237
38. Rausch V, Hackl M, Oppermann J, Leschinger T, Scaal M, Müller LP, et al. Peroneal nerve location at the fibular head: an anatomic study using 3D imaging. *Arch Orthop Trauma Surg* 2019;139:921-926

https://doi.org/10.3348/kjr.2024.0912